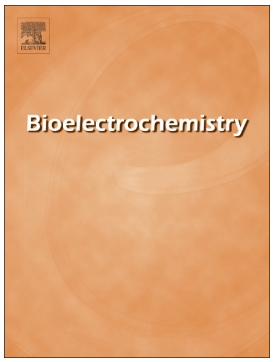

Hydrogen peroxide biosensor based on chitosan/2D layered double hydroxide composite for the determination of H2O2

Jian Yuan, Sheng Xu, Hong-Yan Zeng, Xi Cao, A. Dan Pan, Gao-Fei Xiao, Peng-Xuan Ding

PII: S1567-5394(18)30060-4
DOI: doi:10.1016/j.bioelechem.2018.04.009
Reference: BIOJEC 7145

To appear in: *Bioelectrochemistry*

Received date: 4 February 2018
Revised date: 17 April 2018
Accepted date: 17 April 2018

Please cite this article as: Jian Yuan, Sheng Xu, Hong-Yan Zeng, Xi Cao, A. Dan Pan, Gao-Fei Xiao, Peng-Xuan Ding , Hydrogen peroxide biosensor based on chitosan/2D layered double hydroxide composite for the determination of H2O2. The address for the corresponding author was captured as affiliation for all authors. Please check if appropriate. Biojec(2017), doi:10.1016/j.bioelechem.2018.04.009

Hydrogen Peroxide Biosensor based on Chitosan/2D Layered Double Hydroxide Composite for the Determination of H_2O_2

Jian Yuan, Sheng Xu*, Hong-Yan Zeng*, Xi Cao, A Dan Pan, Gao-Fei Xiao, Peng-Xuan Ding

College of Chemical Engineering, Xiangtan University, Xiangtan, Hunan, 411105, China

*Corresponding Author:

Hong-Yan Zeng

E-mail address: hongyanzeng99@hotmail.com

Tel.: +86-731-58298175

Sheng Xu

E-mail address: xusheng2016@xtu.edu.cn

Address: College of Chemical Engineering, Xiangtan University, Xiangtan, Hunan, 411105, China

Abstract

The composites (LDH-CMC) composed of carboxymethyl chitosan (CMC) and 2D ZnAl layered double hydroxide (LDH) were successfully prepared using the one-step urea method; these composites were characterized by XRD, FT-IR, UV-vis DRS, SEM, BJH/BET, TG-DTG and pH_{zpc} analyses, cyclic voltammetry, and electrochemical impedance spectroscopy. The use of CMC could impact the textural and surface chemical properties of the LDH-CMC composites, where the composites still maintained the 2D layered structure. Incorporating a moderate amount of CMC could increase both the surface area and the permanent charge density of the composites, leading to improved electrochemical performances. The LDH-CMC composite was used as a support matrix for the immobilization of horseradish peroxidase (HRP) on the glass carbon (GC) electrode to construct a biosensor that provides a biocompatible microenvironment for HRP and a pathway for H_2O_2 diffusion via the high surface area. The HRP biosensor displayed a satisfactory sensitivity and fast response (less than 3 s) toward H_2O_2 over a wide linear range of 0.02~6.0 $mmol \cdot L^{-1}$ with a low detection limit of 12.4 $\mu mol \cdot L^{-1}$, good anti-interference ability and long-term storage stability. The proposed HRP biosensor was found to be a sensitive, rapid, and disposable sensor with low cost, easy preparation and high selectivity; thus, the proposed biosensor can be used for the real-time detection of trace H_2O_2 in the biological, clinical and environmental fields.

Keywords: Layered double hydroxide; Carboxymethyl chitosan; Horseradish peroxidase biosensor; H_2O_2.

1. Introduction

Sensitive and selective determination of H_2O_2 is of great significance in biological, clinical, environmental and many other fields [1-3]. Several analytical techniques, such as fluorescence [4], electrochemical [1] and chemiluminescence [5] methods, have been employed for the determination of H_2O_2. Among these methods, electrochemical sensors have attracted much attention because of their low detections limit, high selectivity and sensitivity [1]. In particular, the electrochemical enzyme sensors coupled with the intrinsic selectivity and sensitivity of enzymatic reactions is attractive because of the operational simplicity, low-cost and high sensitivity in fabricating sensitive and linearly responding devices [2,6]. To date, horseradish peroxidase (HRP) has been the most commonly used enzyme for the construction of H_2O_2 biosensors [7,8]. Direct electrochemical reduction of H_2O_2 between HRP and electrode is not effective for analytical application because of the slow electrode kinetics of the denaturation of HRP [9]. Therefore, the effective immobilization of HRP on the electrode surface, as a means to both provide a suitable microenvironment for enzyme proteins and enhance direct electron transfer, is necessary and important in the development of HRP biosensors.

Recent studies found that the immobilization of HRP on layered double hydroxides (LDH) [9], porous graphene [8] and ceramic-carbon [10] exhibited good synergetic effect on H_2O_2 reduction. Of the wide variety of inorganic materials, LDH materials are very attractive as support matrices for the immobilization of enzyme proteins that represents an inexpensive, fast, and easy method to produce enzyme electrodes for the development of electrochemical

sensors. However, their practical applications are limited by the relatively low lifetime of the biosensor arising from the low loading and slow leaching of enzymes [11]. To solve these problems, some composites incorporating organic matters have been prepared to improve the stability and increase the amount of enzymes immobilized on the LDH. These new inorganic-organic composites are particularly important for biosensor fabrication because they can be prepared under ambient conditions and they exhibit high anion-exchange capacity, high thermal and reactive stabilities, chemical inertness, and experience negligible swelling in aqueous solution [12-14]. In particular, the LDH/chitosan composites were found to exhibit better electrocatalytical responses than that of the individual LDH materials [15-18]. Biocompatible chitosan is able to resist against aggregation of the LDH particles, and large quantities of –OH, –COOH and $–NH_3$ in the chitosan chains can also stabilize the activity of the enzyme via the interactions among them [19]. In spite of these improvements in LDH/chitosan materials as a support matrix for immobilization of enzymes and the construction of amperometric biosensors, there is still an emerging need to develop a simple, easy to use and low-cost preparation method to produce an enzyme sensor with high performance. To date, the majority of LDH/chitosan materials are prepared by briefly wrapping chitosan on the surface of the LDHs and then immobilizing the enzyme for biosensing applications; this approach results in relatively poor stability, short lifetime and low bioactivity of enzyme. Therefore, efforts should be made to seek a simple and reliable scheme to prepare a LDH/chitosan material for immobilizing enzyme proteins that overcome these shortcomings.

In the present work, a novel electrochemical horseradish peroxidase (HRP) biosensor was

constructed for the quantitative determination of H_2O_2 based on a HRP/LDH-CMC modified electrode. The LDH-CMC composite (as a support matrix for the HRP immobilization) was successfully synthesized using the urea method, and HRP (selected as a model enzyme) was immobilized on the LDH-CMC composite. To clarify the relationship between the microstructure and electrochemical stability, the physico-chemical properties of the LDH-CMC composites were characterized by XRD, FT-IR, UV-vis DRS, SEM, TG-DTG, BJH/BET and pH_{zpc} measurements. In addition, the analytical performances of the enzyme sensor with respect to electrocatalytic activity, repeatability and stability were evaluated. The HRP biosensor showed high sensitivity, good reproducibility and long-term stability to the reduction of H_2O_2, suggesting that the proposed strategy can be extended to the development of other enzyme-based biosensors.

2. Experimental

2.1. Materials

Carboxymethyl chitosan (CMC, viscosity 10~80 cps and carboxymethyl degree 80%) was purchased from Shanghai Shifeng Biological Technology Co. Ltd, and horseradish peroxidase (HRP, 300 $U \cdot mg^{-1}$) was purchased from Sigma. All chemicals were of analytical grade and purchased from Sinopharm Chemical Reagent Co. Ltd., China. The 0.1 $mol \cdot L^{-1}$ phosphate buffer solutions (PBS) at different pH were prepared by mixing the stock solutions of 0.1 $mol \cdot L^{-1}$ NaH_2PO_4 and 0.1 $mol \cdot L^{-1}$ Na_2HPO_4 with different proportions, and all other solutions were made with deionized water. A pH electrode (Mettler Toledo S40K) was used for pH measurements, and 0.1 $mol \cdot L^{-1}$ KOH and HCl solutions were used for pH adjustment.

2.2. Preparation of Zn/Al layered double hydroxide

For the sake of comparison, the Zn/Al-CO_3^{2-} layered double hydroxide precursor with Zn/Al molar ratio of 3.0 was prepared using the urea method according to the literature previously described [20]. The resulting product, which was denoted as LDH, was obtained by drying at 80°C for 10 h.

2.3. Preparation of the LDH and CMC composites

The LDH and CMC composites were prepared according to the urea method, using CMC molecules as a template. CMC solutions with the CMC concentrations of 1.0, 2.0 and 3.0 $g \cdot L^{-1}$ were separately obtained by dissolving powdered CMC in the solution containing 1.0 wt% acetic acid. During the preparation of the composite, 400 mL mixed salt solution containing $Zn(NO_3)_2 \cdot 6H_2O$ (0.12 $mol \cdot L^{-1}$), $Al(NO_3)_3 \cdot 9H_2O$ (0.04 $mol \cdot L^{-1}$) and urea (urea/NO_3^- molar ratio of 4.0) was placed into a three-neck flask. A total of 100 mL CMC solution was dropped into the mixed salt solution under stirring (300 rpm) at a pH of 8.5 at room temperature. After dripping, the reaction temperature was heated to 105ºC and then maintained for 12 h under stirring. After the reaction, the suspension was crystallized at 80°C for 18 h, filtrated, washed, and then dried at 90°C for 6 h; the final product was denoted as LDH-CMC. For convenience, the resulting products prepared in the CMC solutions of 1.0, 2.0 and 3.0 $g \cdot L^{-1}$ were designated LDH-CMC_1, LDH-CMC_2 and LDH-CMC_3, respectively.

2.4. Preparation of the LDH-CMC modified electrodes

Prior to modification, a glass carbon electrode (GCE, 2 mm in diameter) was carefully polished with 0.3 and 0.05 μm α-Al_2O_3 powders in sequence, rinsed thoroughly with pure water between each polishing step, and then sonicated in ethanol and pure water for 5 min each. After these pretreatments, the cleaned GCE was dried in air. 10 μL of 1.0 $mg{\cdot}mL^{-1}$ active material (LDH, LDH-CMC_1, LDH-CMC_2 or LDH-CMC_3) was dropped onto the surface of the cleaned GCE and then dried under infrared radiation for 3 min to obtain the film modified electrode. The modified electrodes were designated LDH/GCE, LDH-CMC_1/GCE, LDH-CMC_2/GCE and LDH-CMC_3/GCE in sequence.

2.5. Fabrication of the HRP/LDH-CMC biosensor

The LDH-CMC_2 colloidal suspension (2.0 $mg{\cdot}mL^{-1}$) was prepared by ultrasonically dispersing the composite in water for 2 h. HRP solution (2.0 $mg{\cdot}mL^{-1}$) was obtained by dissolving the enzyme in PBS buffer (0.1 $mol{\cdot}L^{-1}$, pH 7.0). According to our preliminary experiments, the critical preparation parameters for preparing the HRP biosensor were examined in the PBS buffer for the response (*i*) to 1 $mmol{\cdot}L^{-1}$ H_2O_2 by current-time curves (see detailed information in Fig. S1). The suitable mass ratio of LDH-CMC_2 to HRP was 1.0, and the HRP/LDH-CMC_2 composite loading was 10 μL. A total of 10 μL LDH-CMC_2 suspension solution was mixed adequately in 10 μL of the HRP solution, and the immobilization reaction of enzyme was conducted under vibration for 6 h. Next, the HRP biosensor was constructed by coating 10 μL of the resulting mixture onto the cleaned GCE; the resulting electrode was designated HRP/LDH-CMC/GCE.

2.6. Measurements of the CV and EIS

Electrochemical measurements of the cyclic voltammetry (CV) and impedance spectroscopy (EIS) were performed with a CHI660D electrochemical workstation (Shanghai Chenhua Apparatus Co. Ltd., Shanghai, China) using the typical setup of a three-electrode electrochemical configuration, with the modified carbon electrode (2 mm in diameter) as the working electrode, and platinum foil and Hg/HgO electrodes as the counter and reference electrodes, respectively.

For the LDH-CMC modified electrodes, CV measurements were conducted in 0.1 $mol \cdot L^{-1}$ KCl, 5 $mmol \cdot L^{-1}$ $K_3[Fe(CN)_6]$ and 5 $mmol \cdot L^{-1}$ $K_4[Fe(CN)_6]$ aqueous electrolyte at room temperature. CV tests were performed between −0.4 and 0.8 V (vs. Hg/HgO) at 100 $mV \cdot s^{-1}$ in the 6^{th} cycle. EIS measurements were performed by applying an AC voltage with 5 mV amplitude in a frequency range from 0.01 to 100 kHz.

For the HRP/LDH-CMC/GCE, CV measurements were performed in an unstirred PBS solution (pH 7.0) at a scan rate of 100 $mV \cdot s^{-1}$ in the 6^{th} cycle. EIS measurements were performed in 0.1 $mol \cdot L^{-1}$ KCl, 5 $mmol \cdot L^{-1}$ $K_3[Fe(CN)_6]$ and 5 $mmol \cdot L^{-1}$ $K_4[Fe(CN)_6]$ aqueous electrolyte by applying an AC voltage with 5 mV in a frequency range from 0.01 to 100 kHz at room temperature. The H_2O_2 limit of detection (LOD, $\mu mol \cdot L^{-1}$) was calculated as follows [21]:

$$LOD = 3s_B/m \qquad (1)$$

where s_B is the standard deviation of the blank measurement, and m is the slope of the calibration curve.

2.7 Characterization of the LDH-CMC composites

X-ray diffraction (XRD) patterns (D/max-2550PC, Rigaku, Tokyo, Japan) were collected with Cu Kα radiation (λ=1.5406 Å). The scan step was $0.0671 \cdot s^{-1}$ with a filament current of 30 mA and a voltage of 40 kV. Fourier transform infrared (FT-IR) spectra (Spectrum One B, Perkin-Elmer, USA)were recorded using the KBr pellet technique. The UV-visible diffuse reflectance spectra (UV-vis DRS) was recorded by a Shimadzu UV2550 spectrophotometer (Shimadzu, Japan). The pore size and pore volume were calculated from the N_2 desorption isotherm according to the Barrett-Joyner-Hallender (BJH) method (NOVA-2200e, Quantachrome, USA), and the specific surface area was calculated according to the Brunauer-Emmett-Teller (BET) method (NOVA-2200e, Quantachrome, USA). Scanning electron microscopy (SEM) images were obtained using a JEOL JSM-6700F instrument (Japan Electron Optics Laboratory, Japan). Thermogravimetric and differential thermal analysis (TG-DTG) (6300, Seiko, Japan) was conducted in a N_2 atmosphere with a heating rate of $10°C \cdot min^{-1}$ under a He stream flowing at $60\ mL \cdot min^{-1}$.

The determination of the pH point of zero charge (pH_{zpc}) of the samples was conducted using the potentiometric titration (PT) method. The pH at pH_{zpc} was determined in NaCl solutions (inert electrolytes) with different concentrations according the literature [22]. The concentrations of H^+ (Γ_{H^+}) and OH^- (Γ_{OH^-}) were calculated, where the crossover point of ($\Gamma_{OH^-} - \Gamma_{H^+}$) ~ pH_{zpc} curves was pH_{zpc}, and the permanent charge density (σ_p, $C \cdot m^{-2}$) at pH_{zpc} was as follows [22]:

$$\sigma_p = F(\Gamma_{OH^-} - \Gamma_{H^+})_{zpc} / S_{BET} \qquad (2)$$

where S_{BET} is the specific surface area ($m^2 \cdot g^{-1}$) of the samples and F is the Faraday constant

(96485 $C \cdot mol^{-1}$).

3. Results and discussion

3.1. Characterization of the LDH-CMC composites

3.1.1. XRD analyses

The powder XRD patterns of the virgin LDH, LDH-CMC_1, LDH-CMC_2 and LDH-CMC_3 composites are shown in Fig. 1A. A typical layered double hydroxide structure with sharp and intense (003), (006), (009), (110) and (113) reflections and broadened (015) and (018) reflections were observed in all the samples, and no other crystalline phases were observed in all the samples. Furthermore, the clearly distinguished reflections of (110) and (113) highlighted that they were typical of highly crystalline layered double hydroxide structures [23]. The interlayer distances (d_{003} approximately 0.75 nm) for the samples were typical of CO_3^{2-} layered double hydroxide [22]. The results revealed that the incorporation of CMC maintained the native layered double hydroxide structures of LDH-CMC_1, LDH-CMC_2 and LDH-CMC_3.

3.1.2. FT-IR analyses

The FT-IR spectra of the virgin LDH, pure CMC, LDH-CMC_1, LDH-CMC_2 and LDH-CMC_3 samples in the region 400~4000 cm^{-1} are displayed in Fig. 1B. In all the samples, the peaks at approximately 3448 cm^{-1} (structural –OH or –NH stretching vibrations) [24] and 1654 cm^{-1} (water bending vibrations or –NH bending vibration in $–NH_2$) [17, 24, 25] were observed, and

the peak at approximately 1366 cm^{-1} was assigned to the vibrational mode of C=O in carboxylic acid or C-OH [26]. For the pure CMC, the peak at 3448 cm^{-1} indicated the presence of –C-OH and –NH stretching vibrations, the peaks at 2912 cm^{-1} correlated to –CH stretching vibration of –CH and $–CH_2$ from CMC [24, 27], and the peak at 1654 cm^{-1} was attributed to the bending vibration of –NH in $–NH_2$ overlapped with the H_2O bending vibration [27, 28]. The peaks at 1426 and 1366 cm^{-1} corresponded to symmetric or asymmetric $–CH_2$ stretching vibration in the pyranose ring and the vibrational mode of –C-OH from CMC [26, 27], respectively, and the peak at 1068 cm^{-1} corresponded to –C-O-C– in pyranose ring [25, 27]. Except for some minor differences, the similarity in the FT-IR spectra of the virgin LDH, LDH-CMC_1, LDH-CMC_2 and LDH-CMC_3 implied the characteristic of typical layered double hydroxides. The peak at approximately 3448 cm^{-1} was attributed to the stretching vibrations of structural –OH groups in the brucite sheets, and the peak at approximately 1654 cm^{-1} was assigned to the bending vibration of the interlayer H_2O or physically adsorbed H_2O. The three peaks at 1366, 769 and 625 cm^{-1} were ascribed to the asymmetrical stretching vibration and the symmetrical stretching vibration of the interlayer CO_3^{2-}. The peak at 556 cm^{-1} was attributed to translation modes of –OH groups from Al^{3+} or Mg^{2+} in its coordination. The peak at approximately 448 cm^{-1} was assigned to a condensed Al-O group or Mg-O group [22]. Compared with the virgin LDH, the new peaks at approximately 2917 (or 2978 cm^{-1}), 1558 (NH-bending vibration in amide group) and 1435 cm^{-1} indicated the presence of the –CH group of –CH and $–CH_2$ in the pyranose ring and the –NH group, and another peak at approximately 1068 cm^{-1} originated from the –C-O-C– group in glycosidic linkage from CMC. The appearance of these peaks suggested that the

CMC molecule was present in LDH-CMC_1, LDH-CMC_2 and LDH-CMC_3.

3.1.3. UV-vis DRS analyses

UV-Vis DRS measurement is a very simple method used to probe the possible changes in molecule structure of materials. The UV-Vis DRS spectra of the virgin LDH, pure CMC, LDH-CMC_1, LDH-CMC_2 and LDH-CMC_3 are given in Fig. 1C. The virgin LDH showed an intense UV absorption band below 240 nm and a weak band absorption band at 250~320 nm without absorption in the visible region, in agreement with the results in the literature [29]. For the pure CMC, the absorption band at ~220 nm due to the π-π* transition associated with –C=O group was attributed to the oligomer from CMC [17], and the absorption band at 220~500 nm was attributed to $n \rightarrow \sigma$* transitions of the $–NH_2$ group and carbonyl or carboxyl groups of $n \rightarrow \pi$* transitions [30, 31]. For the LDH-CMC composites, a weak absorption band was observed at 220~500 nm, demonstrating the characteristic CMC absorption. However, the absorption was very weak, suggesting that CMC molecules were involved in coordination to the metal ion. Moreover, the intensity in the absorption band increased with CMC content in the LDH-CMC composites, suggesting that CMC incorporated into the LDH-CMC composites.

3.1.4. BJH/BET analyses

To further examine the textural characteristic of the samples, BET gas adsorption measurement was used to characterize pore volume (V_P), pore diameter (D_P) and specific surface area (S_{BET}). The adsorption isotherms of the virgin LDH, LDH-CMC_1, LDH-CMC_2 and LDH-CMC_3 are plotted in Fig. 1D. All the isotherms belonged to the typical type IV

isotherm according to the IUPAC classification. For the virgin LDH, the isotherm with typical H3 hysteresis loop in high relative pressure range of 0.70~0.97 P/P_o corresponded to the aggregates of plate-like particles causing slit-like pores with nonuniform size and almost without micropores, as is typical of mesoporous materials [32]. For the LDH-CMC_1, LDH-CMC_2 and LDH-CMC_3 composites, the isotherms with a hysteresis loop between type H3 and H4 started at a low relative pressure (0.02 P/P_o), corresponding to broad pore size distributions and mesoporous structures with some micropores. The transformation from type H3 to the mixed type H3 and H4 suggested that incorporation of CMC might result in the formation of narrower slit-like pores [33]. The formation of micropores could be caused by the presence of a certain amount of the CMC molecules, probably caused by coverage of the CMC molecule along with the presence of micropore structures [34]. As seen from Fig. 1D(inset), the pore size distribution of the virgin LDH was quite broad (2.0~68 nm), with most likely pore size being 12.38 nm, where the smaller mesopores reflected the presence of pores within the brucite sheets and the larger mesopores were associated with the pores formed between stacked laminates. For the composites, the pore size distribution was in the range of 1.72~66 nm, with a few micropores, where the micropores were in the interaction of the CMC molecules with the laminates leading to the filling of the mesopores accompanied by the inherent micropores of the CMC molecules. As seen in Fig. 1D (inset), the corresponding surface areas (S_{BET}) of the composites suggested that the incorporation of the CMC with the functional groups had a small impact on the S_{BET}. The LDH-CMC_2 showed the highest surface area (70 $m^2 \cdot g^{-1}$), possibly because of the well-dispersed particles, whereas the LDH-CMC_3 had the lowest surface area caused by the excess CMC molecules. It was found

that moderate incorporation of CMC could cause an increase in the S_{BET} and revealed the mesoporous nature of the LDH-CMC composites that contained a few micropores.

3.1.5. SEM analyses

To investigate the morphologies of the virgin LDH, LDH-CMC_1, LDH-CMC_2 and LDH-CMC_3, SEM imaging was used (Fig. 2). As shown in Fig. 2, all the samples exhibited the characteristic platelets with irregular edges, in accordance with the typical 2D layered double hydroxide morphology [22]. The SEM results demonstrated that the incorporation of CMC did not influence the morphology of the LDH and indicated that the preservation of the sheet structure (as most unique property of the LDH) might be important for preparing HRP biosensors. The virgin LDH particles were comprised of stacked thin platelets with irregular edges, and the CMC molecules seemed to provide cohesion to the LDH platelets leading to the aggregation of the platelets. The agglomeration of the platelets was attributed to the interactions between the LDH platelets and the CMC molecules. Obviously, CMC had an effect on the microstructure of the LDH-CMC_1, LDH-CMC_2 and LDH-CMC_3 composites. Comparing with the virgin LDH, the particles of LDH-CMC composites demonstrated better dispersion, and the stacking thickness of platelets increased. For the composites prepared with the addition of different amounts of CMC, the particles of the LDH-CMC_2 were the thickest and the distribution of the particles was the most discrete, providing high specific surface area, robust and practical 3D networks.

3.1.6. TG-DTG analyses

Thermogravimetric analysis (TG) is one of the thermal analysis techniques used to measure the physical chemistry properties of a material as a function of temperature or mass loss. The effect of the pure CMC on the LDH-CMC composites was investigated by TG-DTG; the results are shown in Fig. 2. According to Fig. 2 (inset), the pure CMC had two different stages of weight loss, with the first endothermic peak centered at 86°C with weight loss of 1.0% corresponding to the loss of adsorbed and bound water, and the second exothermic peak centered at 302°C with weight loss of 53.0% corresponding to the decomposition of CMC molecule into H_2O, CO_2 and N_2 [35]. The total weight loss of the pure CMC was 68.5 wt% in the whole pyrolysis process. Moreover, the TG-DTG curves of the virgin LDH, LDH-CMC_1, LDH-CMC_2 and LDH-CMC_3 were basically identical, indicating that the microstructures of the virgin LDH and LDH-CMC composites were fundamentally the same. The first endothermic peak at approximately 170°C corresponded to the loss of physisorbed and interlayer water without the collapse of the hydrotalcite structure. The second endothermic peak at approximately285°C was caused by dehydroxylation in the brucite sheets and loss of the interlayer CO_3^{2-} ions [22]. The temperatures of the two endothermic peaks of the composites were higher than those of the virgin LDH because of the presence of CMC molecules, demonstrating the strengthening interaction between CMC molecules and LDH particles that made it difficult to release physisorbed water, interlayer CO_3^{2-} anions, hydroxyls in the brucite sheets and degrade the CMC. The total weight losses of the virgin LDH, LDH-CMC_1, LDH-CMC_2 and LDH-CMC_3 were 30.7, 37.1, 36.1 and 38.9 wt%, respectively. The weight loss of LDH-CMC_2 was the least among the composites, implying that the thermal stability could be facilitated by appropriate incorporation of CMC into the LDH

substrate. The results further verified that CMC molecules existed in the LDH-CMC composites and that moderate incorporation of CMC could heighten the interaction between the LDH and CMC molecules.

3.1.7. pH point of zero charge analyses

The point of zero charge (pH_{zpc}) was used in the determination of the surface charge properties of the samples. The LDH-CMC_2 had the highest pH_{zpc} at 11.39, followed by the LDH-CMC_1 (11.31) and the LDH-CMC_3 (11.30); the virgin LDH possessed the lowest pH_{zpc} at 11.25 (see detailed information in Fig. S2). A similar trend in the permanent charge density (σ_p) was found, where the σ_p values of the LDH-CMC_2, LDH-CMC_1, LDH-CMC_3 and virgin LDH were 3.67, 3.56, 3.54 and 3.52 $C \cdot m^{-2}$, respectively. The shifts in pH_{zpc} and σ_p of the composites to higher values were believed to be linked with the incorporation of CMC molecules. The results showed that the LDH-CMC composites carried a positive charge below pH 11.3, whereas they carried a negative charge above pH 11.4.

3.2. Electrochemical behavior of the LDH-CMC composites

3.2.1. CV behaviors

The CV curves of LDH/GCE, LDH-CMC_1/GCE, LDH-CMC_2/GCE and LDH-CMC_3/GCE obtained at a scan rate of 100 $mV \cdot s^{-1}$ in the 6^{th} cycle are shown in Fig. 3A. The CV curve of each sample demonstrated that the electrode was charged and discharged at a constant scan rate over the complete cycle with a couple of well-defined redox peaks, suggesting a quasi-reversible electrode process. The anodic and cathodic peaks corresponded to the

oxidation and reduction peaks of $[Fe(CN)_6]^{3-/4-}$ and $Zn(OH)_4^{2-}$ and $Zn(OH)_3^{-}$ couples [36-38]. Compared with the virgin LDH, the peak separation values (ΔE_p) of the LDH-CMC composites showed a diminution, and the ratios of anodic to cathodic peak currents (I_{pa}/I_{pc}) were closer to 1.0 (Fig. 3A). It was clear that the reversibility of the electrochemical transfer was expedited when the CMC molecules were incorporated with the LDH substrate. In particular, the LDH-CMC_2 composite had the smallest ΔE_p value and the I_{pa}/I_{pc} value closest to 1.0, implying that it had the fastest reversible faradic redox reaction due to large available surface area and high charge density. The results indicated the superiority of the LDH-CMC composites (especially LDH-CMC_2 composite) with good reversibility and high sensitivity; thus, the CMC had the ability to promote the electron transfer rate between the LDH and electrode.

To further study the stability of the LDH-CMC_2 composite, the cycle stability was investigated over 50 cycles; the results are shown in the inset of Fig. 3A. Subsequent CV scans showed that the anodic and cathodic peak areas remained almost constant within 50 cycles, and there was very little change between the peak shapes as well as the magnitudes in each cycle after 50 cycles (data not shown), indicating the excellent long-term stability of the LDH-CMC_2/GCE. Furthermore, the CV at different scan rates (v) was also used to determine the electrochemical properties of the LDH-CMC_2/GCE (see detailed information in Fig. S3). The increased ΔE_p value with the increase of scan rate exhibited a quasi-reversible process that the redox reversibility of the LDH-CMC_2 was impaired with the increasing scan rate. Alternatively, the shape of the CV curves was almost maintained with the change of scan rate, demonstrating the good stability of the LDH-CMC_2/GCE electrode. The redox peak current

density (j) increased gradually with the increase of scan rate in the range from 20 to 140 $mV \cdot s^{-1}$. A linear behavior of i_p versus $v^{1/2}$ was obtained (Fig. S3, inset), revealing that the electrode reaction was controlled by the diffusion of $[Fe(CN)_6]^{3-/4-}$ ions.

3.2.2. EIS analyses

For greater understanding, EIS measurements were conducted at open circuit potential; the impedance spectra are shown in Fig. 3B. The Nyquist plots consisted of a semicircular part and a linear part. The semicircular part at higher frequencies corresponds to the electron transfer limited process, with the diameter being equivalent to the electron transfer resistance (R_{et}), while the linear part at lower frequencies corresponds to the diffusion process. After the incorporation of CMC, the value of R_{et} decreased, indicating that the CMC could improve the diffusion of $[Fe(CN)_6]^{3-/4-}$ ions toward the electrode surface. Furthermore, the value of R_{et} of the LDH-CMC_2/GCE electrode was the lowest among the three LDH-CMC/GCE electrodes, implying that the LDH-CMC_2 facilitated the electron-transfer process more effectively than the other two LDH-CMC/GCE electrodes, i.e., the LDH-CMC_2/GCE had the best electrocatalytic activity. The results were in excellent agreement with the CV results, clearly suggesting that the LDH-CMC_2/GCE had highest reversibility of the charge/discharge reaction. According to the characterizations and experiments on electrochemical behavior, the LDH-CMC_2 composite was chosen as the support matrix for the HRP immobilization to construct HRP biosensor for further investigation.

3.3. Electrochemical performances of the HRP biosensor

The main objective of the present work was to utilize the HRP/LDH-CMC_2 film to modify GC electrode for the electrochemical determination of H_2O_2. The experimental parameters, such as initial pH, applied potential, loading of the HRP/LDH-CMC_2, and mass ratio of the LDH-CMC_2 to HRP, were examined by current-time curves; the results are shown in Fig. S1. According to the results, the suitable conditions were as follows: initial pH of 7.0, applied potential of −0.3 V, HRP/LDH-CMC_2 loading of 10 μL and 1.0 mass ratio of LDH-CMC_2 to HRP (see detailed information in Fig. S1).

3.3.1. EIS performance of the HRP/LDH-CMC biosensor

EIS can provide useful information of the impedance changes on the electrode surface between each step. The Nyquist plot of the impedance spectroscopy of the HRP/LDH-CMC/GCE in the presence of equimolar $[Fe(CN)_6]^{3-/4-}$ is shown in Fig. 3B. When the HRP/LDH-CMC film was applied to modify the GCE, a higher R_{et} was obtained via the hindrance of the macromolecular structure of HRP protein to the electron transfer. A significant increase in the interfacial resistance was observed compared with the LDH-CMC_2/GCE. The increase of R_{et} could be attributed to the synergism of HRP and the LDH-CMC_2 matrix. All these results indicated that HRP/LDH-CMC film was successfully assembled on the GCE surface and that the HRP was tightly immobilized onto the LDH-CMC_2 composite.

3.3.2. Electrocatalytic reduction of H_2O_2

The electrocatalytic performances of the HRP/LDH-CMC/GCE in the reduction of H_2O_2 were

investigated by cyclic voltammetry (CV); the results are shown in Fig. 4. The reduction peak current was found to increase with the increase in concentration of H_2O_2 from 0 to 7 mmol·L^{-1}, displaying a typical electrocatalytic reduction process of H_2O_2. Moreover, no direct redox peak was observed for the HRP-free LDH-CMC_2/GCE under the same conditions with the addition of H_2O_2. Thus, the activation energy of H_2O_2 reduction was decreased by the enzymatic catalytic behavior of HRP on the electrode. This result further confirmed that the LDH-CMC_2 composite film provided a friendly platform for the immobilization of HRP, leading to an excellent electrocatalytic activity of the HRP/LDH-CMC for H_2O_2 reduction.

3.3.3. Amperometric biosensing of H_2O_2

Fig. 5A shows a typical current-time plot of the HRP/LDH-CMC/GCE upon the successive addition of 1.0 mmol·L^{-1} H_2O_2 during each 50 s at −0.3 V under the suitable conditions (see detailed information in Fig. S1). The biosensor reached 95% of the steady-state current within 3 s, suggesting a fast response process in the HRP/LDH-CMC/GCE. The HRP biosensor was faster than those reported for the HRP biosensor (5 s) [39] and HRP biosensor (4 s) [40]; similar results (3 s) were also described for HRP biosensors in the literature [41,42]. The response current of the HRP/LDH-CMC/GCE elevated markedly along with H_2O_2 concentration. As shown in Fig. 5A (inset), the biosensor had a wide linear range from 0.02 to 6.0 mmol·L^{-1} (R^2 0.999); this range was wider than those of HRP biosensors for H_2O_2 detection [42,43]. The detection limit (LOD) and sensitivity of the biosensor was estimated to be 12.4 μmol·L^{-1} (S/N=3) and 220.4 μA·(mmol·cm^2)$^{-1}$, respectively. The high sensitivity and wide linear range could be ascribed to the excellent electrocatalytic activity of the

LDH-CMC_2 composite and the biocompatible microenvironment around the HRP protein. A large number of hydrogen bonds in the CMC molecules is favorable to maintain the active configuration of HRP molecules. Moreover, the analytical performances of the HRP biosensor were compared with those H_2O_2 biosensors, as summarized in Table 1; the performances of HRP/LDH-CMC/GCE in the work were found to be comparable to the performances of the H_2O_2 biosensors [42,44,45], with a relatively low detection limit and a wide linear range obtained for the HRP/LDH-CMC system.

When the H_2O_2 concentration was higher than 6.0 mmol·L^{-1}, a plateau current was observed, revealing the characteristics of Michaelis-Menten kinetics. Based on the data obtained in the present study (Fig. 5A), the apparent Michaelis-Menten constant (K_m) was calculated according to Eq.(3), which is applicable for the amperometric biosensors [46]:

$$\frac{1}{i} = \frac{K_m}{i_{max} C} + \frac{1}{i_{max}} \qquad (3)$$

where i is the steady-state current, C is the concentration of H_2O_2, K_m is the apparent Michaelis-Menten constant, and i_{max} is the maximum current.

The K_m value was calculated to be 11.57 mmol·L^{-1} for the HRP/LDH-CMC/GCE (R^2 0.997); this value was smaller than 22.38 mmol·L^{-1} for the HRP biosensor [10], 23.15 mmol·L^{-1} for the HRP biosensor [43] and 21.4 mmol·L^{-1} for the HRP biosensor [47]. The lower K_m value further confirmed that the HRP immobilized on the LDH-CMC_2 composite had higher enzymatic activity, exhibiting higher affinity to H_2O_2, suggesting that the LDH-CMC_2 composite was favorable to maintain the activity of the HRP. The synergistic action of HRP

and LDH-CMC_2 composite allowed the biosensor to exhibit excellent electrocatalytic activity.

3.3.4. Reproducibility and stability of the HRP biosensor

The repeatability was first evaluated through the current response to 1.0 mmol·L^{-1} H_2O_2 for 10 successive determinations using the same HRP biosensor; the relative standard deviation (RSD) was found to be 1.95%, which indicated a satisfactory precision. In the following, the reproducibility of the HRP biosensor was examined with three measurements of 1.0 mmol·L^{-1} H_2O_2 solution using ten different electrodes. The relative standard deviation (RSD) was calculated as 2.15%, suggesting a good replicability. In the end, the stability of the HRP biosensor was also examined during storage in a drying state at 4°C and measured at intervals of a week; it lost only 3.8% of the original value after 1 week, 6.9% of the original value after 2 week, and maintained more than approximately 80.4% of the response after storage for over 1 month. The stability was higher than those in the literature [48,49], indicating the ability of long-term storage and operational stability for the HRP biosensor. The long-term stability could be attributed to good biocompatibility of the LDH-CMC_2 and strong interaction between HRP and LDH-CMC_2.

3.3.5. Selectivity of the HRP biosensor

To investigate the effect of some possible interfering substances on the HRP biosensor, the selectivity and anti-interference ability of the HRP/LDH-CMC/GCE was tested to detect some interfering substances, such as NaCl, KCl, Glucose (Glu), uric acid (UA), ascorbic acid (AA) and dopamine (DA). As shown in Fig. 5B, the successive addition of each interfering

substance in the PBS buffer (pH 7.0) caused a hardly discernible current response, whereas a well-defined H_2O_2 response was obtained, demonstrating good ability of anti-interference to the interfering substances and good selectivity toward H_2O_2.

4. Conclusion

A novel biocompatible composite (LDH-CMC) composed of 2D ZnAl layered double hydroxide (LDH) and carboxymethyl chitosan (CMC)that combined the advantages of inorganic material (LDH) and biomacromolecule (CMC) was successfully synthesized using a simple one-step urea method. The LDH-CMC_2 composite was used as a support matrix to immobilize HRP to construct a H_2O_2 biosensor without the addition of any mediator. The 2D hierarchical porous structure of the LDH-CMC associated with sufficient active sites not only increases the immobilized HRP amount but also provides a biocompatible microenvironment for HRP and a pathway for H_2O_2 diffusion. The resulting HRP/LDH-CMC/GCE exhibited excellent performances, such as satisfactory sensitivity and good stability for quick and specific detection of H_2O_2, implying that the composite could also conveniently extend to the immobilization of other biomolecules and be further developed for other applications.

Acknowledgments

This work is supported by the Joint Research Program of Hunan Provincial Natural Science Foundation (Xiangtan) of China (2016JJ5030), Hunan 2011 Collaborative Innovation Center of Chemical Engineering & Technology with Environmental Benignity and Effective

Resource Utilization and General project of Hunan Provincial Education Department (17C1526) and Ph.D Startup Foundation of Xiangtan University (17QDZ05).

Reference

[1] A.A. Ensafi, M. Jafari-Asl, N. Dorostkar, M. Ghiaci, M.V. Martínez-Huerta, J. Fierro, The fabrication and characterization of Cu-nanoparticle immobilization on a hybrid chitosan derivative-carbon support as a novel electrochemical sensor: application for the sensitive enzymeless oxidation of glucose and reduction of hydrogen peroxide, J. Mater. Chem. B. 2 (2014) 706-717.

[2] K. Yamamoto, T. Ohgaru, M. Torimura, H. Kinoshita, K. Kano, T. Ikeda, Highly-sensitive flow injection determination of hydrogen peroxide with a peroxidase-immobilized electrode and its application to clinical chemistry, Anal. Chimi. Acta. 406 (2000) 201-207.

[3] M. Farrokhnia, S. Karimi, S. Momeni, S. Khalililaghab, Colorimetric sensor assay for detection of hydrogen peroxide using green synthesis of silver chloride nanoparticles: Experimental and theoretical evidence, Sensor. Actuat. B Chem. 246 (2017) 979-987.

[4] C. Liu, Y. Ding, Q. Li, Y. Lin, Photochemical synthesis of glutathione-stabilized silver nanoclusters for fluorometric determination of hydrogen peroxide, Microchim. Acta. (2017) 1-7.

[5] O.S. Wolfbeis, A. Dürkop, M. Wu, Z. Lin, A europium‐ion‐based luminescent sensing probe for hydrogen peroxide, Angew. Chem. Int. Edit. 41 (2002) 4495-4498.

[6] B. Wang, B. Li, Z. Wang, G. Xu, Q. Wang, S. Dong, Sol−Gel thin-film immobilized soybean peroxidase biosensor for the amperometric determination of hydrogen peroxide in acid medium, Anal. Chem. 71 (1999) 1935-1939.

[7] T. Tatsuma, Y. Okawa, T. Watanabe, Enzyme monolayer-and bilayer-modified tin oxide electrodes for the determination of hydrogen peroxide and glucose, Anal. Chem. 61 (1989) 2352-2355.

[8] Y. Liu, X. Liu, Z. Guo, Z. Hu, Z. Xue, X. Lu, Horseradish peroxidase supported on porous graphene as a novel sensing platform for detection of hydrogen peroxide in living

cells sensitively, Biosens. Bioelectron. 87 (2017) 101-107.

[9] X. Chen, C. Fu, Y. Wang, W. Yang, D.G. Evans, Direct electrochemistry and electrocatalysis based on a film of horseradish peroxidase intercalated into Ni–Al layered double hydroxide nanosheets, Biosens. Bioelectron. 24 (2008) 356-361.

[10] H. Chen, S. Dong, Direct electrochemistry and electrocatalysis of horseradish peroxidase immobilized in sol–gel-derived ceramic–carbon nanotube nanocomposite film, Biosens. Bioelectron. 22 (2007) 1811-1815.

[11] C. Mousty, Sensors and biosensors based on clay-modified electrodes—new trends, Appl. Clay Sci. 27 (2004) 159-177.

[12] Y. Xu, X. Liu, Y. Ding, L. Luo, Y. Wang, Y. Zhang, Y. Xu, Preparation and electrochemical investigation of a nano-structured material Ni^{2+}/MgFe layered double hydroxide as a glucose biosensor, Appl. Clay Sci. 52 (2011) 322-327.

[13] Y.-T. Zhang, T.-T. Zhi, L. Zhang, H. Huang, H.-L. Chen, Immobilization of carbonic anhydrase by embedding and covalent coupling into nanocomposite hydrogel containing hydrotalcite, Polymer 50 (2009) 5693-5700.

[14] D. Shan, S. Cosnier, C. Mousty, HRP/[Zn–Cr–ABTS] redox clay-based biosensor: design and optimization for cyanide detection, Biosens. Bioelectron. 20 (2004) 390-396.

[15] H. Ai, X. Huang, Z. Zhu, J. Liu, Q. Chi, Y. Li, Z. Li, X. Ji, A novel glucose sensor based on monodispersed Ni/Al layered double hydroxide and chitosan, Biosens. Bioelectron. 24 (2008) 1048-1052.

[16] E. Han, D. Shan, H. Xue, S. Cosnier, Hybrid material based on chitosan and layered double hydroxides: characterization and application to the design of amperometric phenol biosensor, Biomacromolecules 8 (2007) 971-975.

[17] L. Luo, Q. Li, Y. Xu, Y. Ding, X. Wang, D. Deng, Y. Xu, Amperometric glucose biosensor based on $NiFe_2O_4$ nanoparticles and chitosan, Sensor. Actuat. B Chem. 145 (2010) 293-298.

[18] L. Luo, L. Zhu, Y. Xu, L. Shen, X. Wang, Y. Ding, Q. Li, D. Deng, Hydrogen peroxide biosensor based on horseradish peroxidase immobilized on chitosan-wrapped NiFe2O4 nanoparticles, Microchim. Acta. 174 (2011) 55-61.

[19] L. Fan, Y. Du, B. Zhang, J. Yang, J. Zhou, J.F. Kennedy, Preparation and properties of alginate/carboxymethyl chitosan blend fibers, Carbohyd. Polym. 65 (2006) 447-452.

[20] H.Y. Zeng, X. Deng, Y.J. Wang, K.B. Liao, Preparation of Mg-Al hydrotalcite by urea method and its catalytic activity for transesterification, AIChE J. 55 (2009) 1229-1235.

[21] G.L. Long, J.D. Winefordner, Limit of detection. A closer look at the IUPAC definition, Anal Chem. 55 (1983) 712A-724A.

[22] S. Xu, M.-C. Liao, H.-Y. Zeng, Z.-Q. Zhang, X.-J. Liu, P.-H. Zhu, Ultrafine hydrotalcite particles prepared with novel technology to improve the flame retardancy of polypropylene, Appl. Clay Sci. 108 (2015) 215-221.

[23] F. Cavani, F. Trifirò, A. Vaccari, Hydrotalcite-type anionic clays: Preparation, properties and applications, Catal. Today. 11 (1991) 173-301.

[24] N. Viswanathan, S. Meenakshi, Enriched fluoride sorption using alumina/chitosan composite, J. Hazard. Mater. 178 (2010) 226-232.

[25] M. Darder, M. Colilla, E. Ruiz-Hitzky, Biopolymer–clay nanocomposites based on chitosan intercalated in montmorillonite, Chem. Mater. 15 (2003) 3774-3780.

[26] Y. Si, E.T. Samulski, Synthesis of water soluble graphene, Nano Lett. 8 (2008) 1679-1682.

[27] A. Pawlak, M. Mucha, Thermogravimetric and FTIR studies of chitosan blends, Thermochim. Acta 396 (2003) 153-166.

[28] M. Darder, M. Colilla, E. Ruiz-Hitzky, Chitosan–clay nanocomposites: application as electrochemical sensors, Appl. Clay Sci. 28 (2005) 199-208.

[29] W. Zhou, Y. Chen, J. Qian, F. Sun, M. He, Q. Chen, Copper Tetrasulfophthalocyanine Intercalated Hydrotalcite as an Efficient Bifunctional Catalyst for the Baeyer-Villiger

Oxidation, Catal. Lett. 146 (2016) 2157-2164.

[30] S.-M. Wang, Q.-Z. Huang, Q.-S. Wang, Study on the synergetic degradation of chitosan with ultraviolet light and hydrogen peroxide, Carbohyd. Res. 340 (2005) 1143-1147.

[31] M. Nawi, A.H. Jawad, S. Sabar, W.W. Ngah, Photocatalytic-oxidation of solid state chitosan by immobilized bilayer assembly of TiO_2-chitosan under a compact household fluorescent lamp irradiation, Carbohyd. Polym. 83 (2011) 1146-1152.

[32] K. Parida, L. Mohapatra, N. Baliarsingh, Effect of Co^{2+} substitution in the framework of carbonate intercalated Cu/Cr LDH on structural, electronic, optical, and photocatalytic properties, J. Phys. Chem. C. 116 (2012) 22417-22424.

[33] K.S. Sing, Reporting physisorption data for gas/solid systems with special reference to the determination of surface area and porosity (Recommendations 1984), Pure Appl. Chem. 57 (1985) 603-619.

[34] C. Kresge, M. Leonowicz, W. Roth, J. Vartuli, J. Beck, Ordered mesoporous molecular sieves synthesized by a liquid-crystal template mechanism, Nature 359 (1992) 710-712.

[35] A.A. Aghzzaf, B. Rhouta, J. Steinmetz, E. Rocca, L. Aranda, A. Khalil, J. Yvon, L. Daoudi, Corrosion inhibitors based on chitosan-heptanoate modified beidellite, Appl. Clay Sci. 65 (2012) 173-178.

[36] X. Fan, Z. Yang, R. Wen, B. Yang, W. Long, The application of Zn-Al-hydrotalcite as a novel anodic material for Ni-Zn secondary cells, J. Power Sources. 224 (2013) 80-85.

[37] Y. Yuan, J. Tu, H. Wu, C. Zhang, S. Wang, X. Zhao, Influence of surface modification with Sn 6 O 4 (OH) 4 on electrochemical performance of ZnO in Zn/Ni secondary cells, J. Power Sources. 165 (2007) 905-910.

[38] J. Han, H.-Y. Zeng, X. Cao, C.-R. Chen, Cycling stability of iron-based layered double hydroxide thin-films for battery-type electrode materials, J. Mater. Sci. Mater. El. 28 (2017) 2754-2762.

[39] Q. Xu, C. Mao, N.-N. Liu, J.-J. Zhu, J. Sheng, Direct electrochemistry of horseradish

peroxidase based on biocompatible carboxymethyl chitosan-gold nanoparticle nanocomposite, Biosens. Bioelectron. 22 (2006) 768-773.

[40] H. Dai, W. Lü, X. Zuo, Q. Zhu, C. Pan, X. Niu, J. Liu, H. Chen, X. Chen, A novel biosensor based on boronic acid functionalized metal-organic frameworks for the determination of hydrogen peroxide released from living cells, Biosens. Bioelectron. 95 (2017) 131-137.

[41] K. Zhou, Y. Zhu, X. Yang, J. Luo, C. Li, S. Luan, A novel hydrogen peroxide biosensor based on Au–graphene–HRP–chitosan biocomposites, Electrochim. Acta 55 (2010) 3055-3060.

[42] X. Yang, F. Xiao, H. Lin, F. Wu, D. Chen, Z. Wu, A novel H_2O_2 biosensor based on Fe_3O_4-Au magnetic nanoparticles coated horseradish peroxidase and graphene sheets-Nafion film modified screen-printed carbon electrode, Electrochim. Acta 109 (2013) 750-755.

[43] X. Zhao, Z. Mai, X. Kang, X. Zou, Direct electrochemistry and electrocatalysis of horseradish peroxidase based on clay-chitosan-gold nanoparticle nanocomposite, Biosens. Bioelectron. 23 (2008) 1032-1038.

[44] S. Farzana, V. Ganesh, S. Berchmans, A Sensing Platform for Direct Electron Transfer Study of Horseradish Peroxidase, J. Electrochem. Soc. 160 (2013) H573-H580.

[45] D.A. Centeno, X.H. Solano, J.J. Castillo, A new peroxidase from leaves of guinea grass (*Panicum maximum*): A potential biocatalyst to build amperometric biosensors, Bioelectrochemistry 116 (2017) 33-38.

[46] Y. Zou, C. Xiang, L.-X. Sun, F. Xu, Glucose biosensor based on electrodeposition of platinum nanoparticles onto carbon nanotubes and immobilizing enzyme with chitosan-SiO_2 sol-gel, Biosens. Bioelectron. 23 (2008) 1010-1016.

[47] X. Tan, J. Zhang, S. Tan, D. Zhao, Z. Huang, Y. Mi, Z. Huang, Amperometric hydrogen peroxide biosensor based on horseradish peroxidase immobilized on Fe_3O_4/chitosan modified glassy carbon electrode, Electroanalysis 21 (2009) 1514-1520.

[48] Y. Wang, Z. Wang, Y. Rui, M. Li, Horseradish peroxidase immobilization on carbon nanodots/CoFe layered double hydroxides: direct electrochemistry and hydrogen peroxide sensing, Biosens. Bioelectron. 64 (2015) 57-62.

[49] L. Ma, R. Yuan, Y. Chai, S. Chen, Amperometric hydrogen peroxide biosensor based on the immobilization of HRP on DNA-silver nanohybrids and PDDA-protected gold nanoparticles, J. Mol. Catal. B Enzym. 56 (2009) 215-220.

Table 1 Comparison with the analytical performance of other biosensors for H_2O_2 determination.

Sensor	Potential (V)	Linear range ($\mu mol \cdot L^{-1}$)	LOD ($\mu mol \cdot L^{-1}$)	Ref.
SPCE/GS-Nafion/Fe_3O_4-Au-HRP*	−0.3	20~2500	12	[42]
Clay-HRP-Clay/AuCS*	−0.2	39~3100	9	[43]
PGG/GS*	−0.65	100~4000	150	[45]
Dendrimer/Au/CS/HRP/ITO*	−0.28	165~1500	200	[46]
HRP/LDH-CMC	−0.3	20~6000	12.4	This work

*SPCE: screen-printed carbon electrode; GS: graphene sheets; AuCS: chitosan-Au nanoparticles nanocomposite; PGG: Peroxidases from leaves of Guinea grass; CS: chitosan; ITO: indium tin oxide.

Highlights

1.LDH-CMC was prepared using the one-step urea method.

2. Incorporation of moderate amount of CMC into the LDH (LDH-CMC_2) could increase the electrochemical performances.

3. H_2O_2 biosensor has fast response (less than 3 s), LOD: 12.4 μmol·L^{-1} and linear range: 0.02~6.0 mmol·L^{-1}.

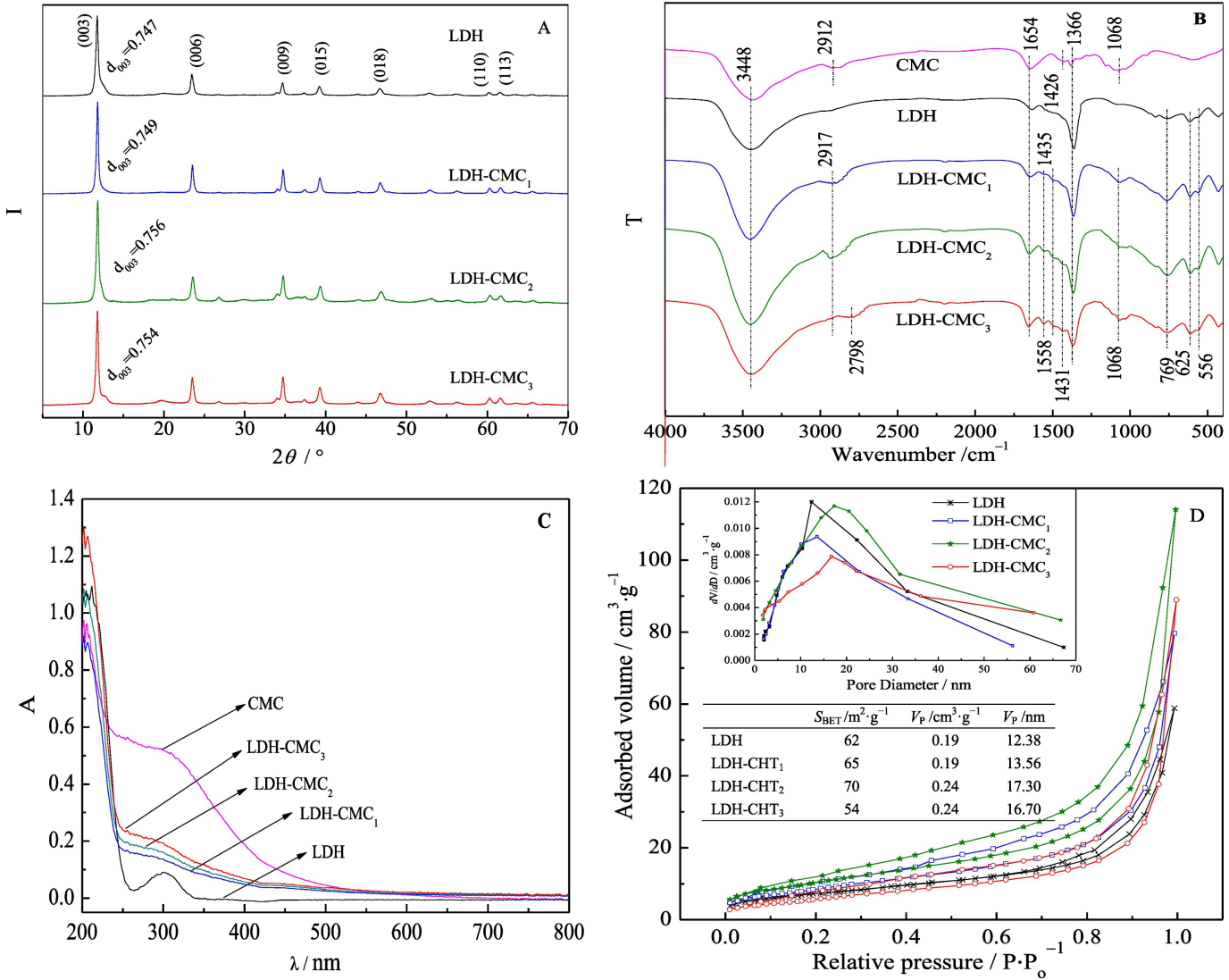

	S_{BET} /m^2·g^{-1}	V_P /cm^3·g^{-1}	V_P /nm
LDH	62	0.19	12.38
LDH-CHT$_1$	65	0.19	13.56
LDH-CHT$_2$	70	0.24	17.30
LDH-CHT$_3$	54	0.24	16.70

Figure 1

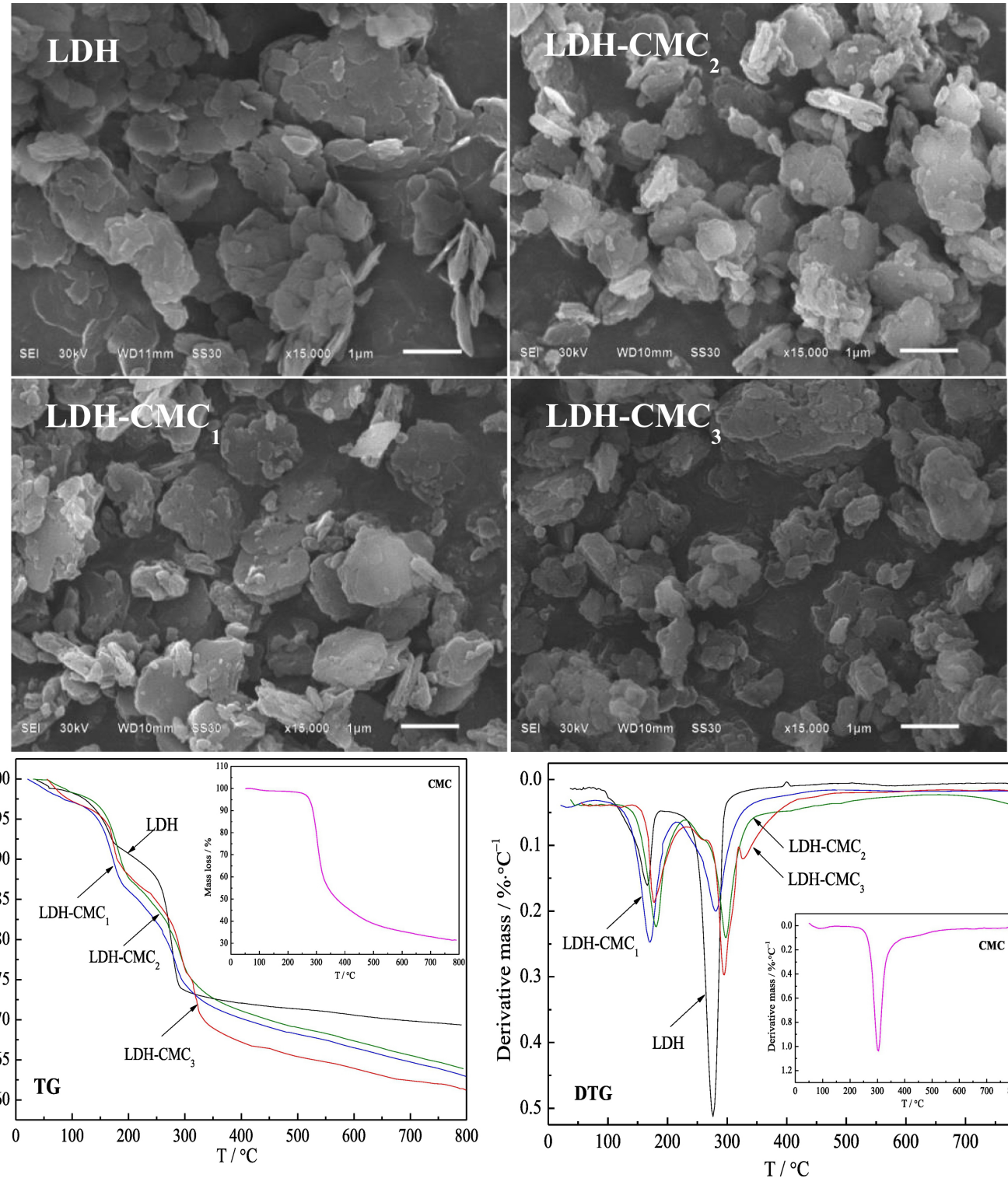
LDH
LDH-CMC2
LDH-CMC1
LDH-CMC3
SEI 30kV WD11mm SS30 x15,000 1μm
SEI 30kV WD10mm SS30 x15,000 1μm
SEI 30kV WD10mm SS30 x15,000 1μm
SEI 30kV WD10mm SS30 x15,000 1μm
Mass loss / %
T / °C
TG
LDH
LDH-CMC1
LDH-CMC2
LDH-CMC3
CMC
Mass loss / %
T / °C
Derivative mass / %·°C−1
T / °C
DTG
LDH-CMC2
LDH-CMC3
LDH-CMC1
LDH
CMC
Derivative mass / %·°C−1
T / °C

Figure 2

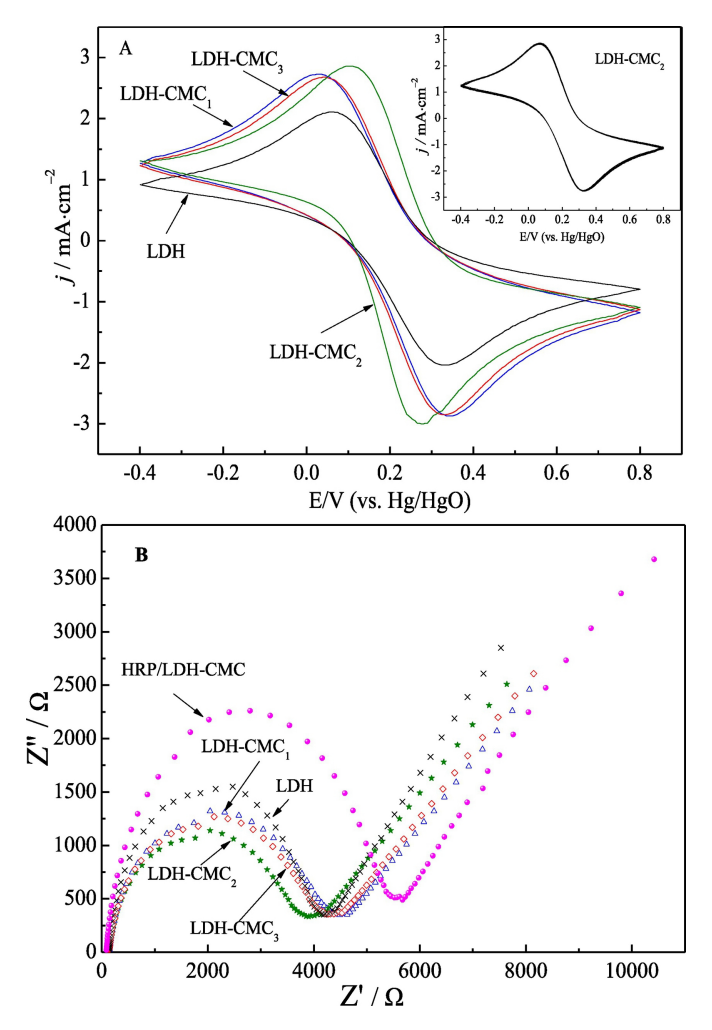
A
LDH-CMC3
LDH-CMC1
LDH
LDH-CMC2
j / mA·cm-2
E/V (vs. Hg/HgO)
LDH-CMC2
B
HRP/LDH-CMC
LDH-CMC1
LDH
LDH-CMC2
LDH-CMC3
Z'' / Ω
Z' / Ω

Figure 3

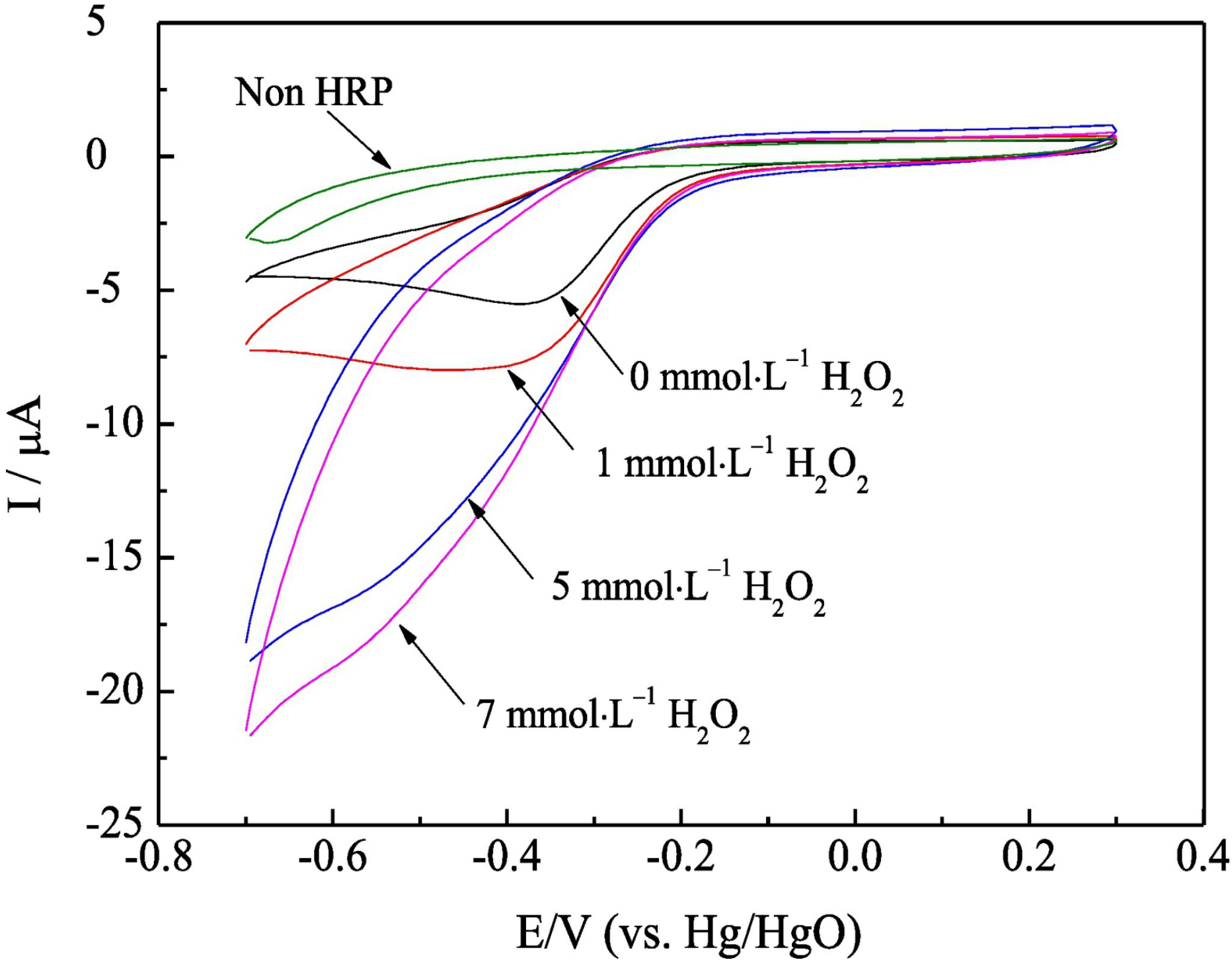
Non HRP
0 mmol·L^{-1} H_2O_2
1 mmol·L^{-1} H_2O_2
5 mmol·L^{-1} H_2O_2
7 mmol·L^{-1} H_2O_2
I / μA
E/V (vs. Hg/HgO)
5
0
-5
-10
-15
-20
-25
-0.8
-0.6
-0.4
-0.2
0.0
0.2
0.4

Figure 4

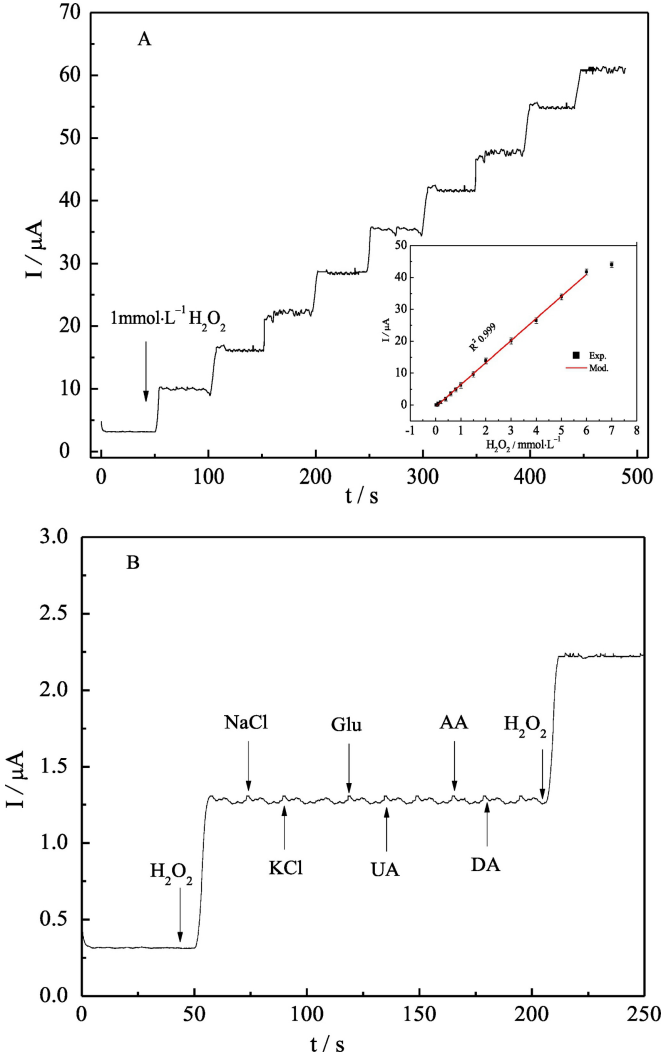
A
I / μA
t / s
1mmol·L⁻¹ H2O2
R² 0.999
Exp.
Mod.
I / μA
H2O2 / mmol·L⁻¹
B
I / μA
t / s
H2O2
NaCl
KCl
Glu
UA
AA
DA
H2O2

Figure 5